Global and Planetary Change 131 (2015) 115–123

Contents lists available at ScienceDirect

Global and Planetary Change

journal homepage: www.elsevier.com/locate/gloplacha

Water availability change in central Belgium for the late 21st century

Hossein Tabari [a,*], Meron Teferi Taye [a], Patrick Willems [a,b]

[a] Hydraulics Division, Department of Civil Engineering, KU Leuven, Kasteelpark Arenberg 40, BE-3001 Leuven, Belgium
[b] Department of Hydrology and Hydraulic Engineering, Vrije Universiteit Brussel, Belgium

ARTICLE INFO

Article history:
Received 9 March 2015
Received in revised form 13 May 2015
Accepted 18 May 2015
Available online 24 May 2015

Keywords:
Water balance
Precipitation
Evapotranspiration
Climate change
CMIP5 models

ABSTRACT

We investigate the potential impact of climate change on water availability in central Belgium. Two water balance components being precipitation and potential evapotranspiration are initially projected for the late 21st century (2071–2100) based on 30 Coupled Models Intercomparison Project phase 5 (CMIP5) models relative to a baseline period of 1961–1990, assuming forcing by four representative concentration pathway emission scenarios (RCP2.6, RCP4.5, RCP6.0, RCP8.5). The future available water is then estimated as the difference between precipitation and potential evapotranspiration projections. The number of wet days and mean monthly precipitation for summer season is projected to decrease in most of the scenarios, while the projections show an increase in those variables for the winter months. Potential evapotranspiration is expected to increase during both winter and summer seasons. The results show a decrease in water availability for summer and an increase for winter, suggesting drier summers and wetter winters for the late 21st century in central Belgium.

1. Introduction

The great significance of water resources for sustainable development underscores the necessity of understanding how much more or less water will be available in the future under climate change. Evaluation of climate change impact on the balance between water availability and water demand is more important at regional scale because global precipitation may show an increasing trend for the future, while some regions suffer severely from decreased precipitation along with increased evapotranspiration. Although precipitation and river runoff for high latitudes are projected to increase (Cisneros et al., 2014); however, how climate change will affect water availability in individual seasons provides a good guide to improve water management practices to cope with possible damages of seasonal flood and drought in the future and to secure the sustainability of water supplies. Nevertheless, while climate change effect on water availability and water demand is significant in some regions, it is not the only factor in play. Non-climatic factors such as population growth and growing demand for water over the coming decades will put further pressure on available water resources and exacerbate the problems with making current water management systems unreliable for the future. The traditional approach for water resource designing and planning with the assumption "the characteristics of the future events will resemble the past" is not applicable anymore (Milly et al., 2008; Lins and Cohn, 2011; Matalas, 2012) because of observed non-stationarity in hydrological variables and climate change impacts (Kling et al., 2014).

Changes in water availability will depend on the changes in precipitation and evapotranspiration as two key components of the hydrological cycle (Bates et al., 2008). The periods and quantities of water surplus and water deficit are determined by comparing precipitation and potential evapotranspiration values (Shifteh Some'e et al., 2013; Tabari and Aghajanloo, 2013; Tabari and Hosseinzadeh Talaee, 2013). The difference between precipitation and evapotranspiration is indeed a measure of sustainable water availability (Milly et al., 2005). However, the effect of climate change on these variables is uncertain in particular when it comes to change in extreme values. A significant part of this uncertainty arises from climate model projections that disagree on the magnitude of change and in some cases even on the direction (Meehl et al., 2007; Schewe et al., 2014). Recently, a new generation of General Circulation Models (GCMs) from the Coupled Model Intercomparison Project Phase 5 (CMIP5) has been released to reduce projection uncertainty related to CMIP3 GCMs and has become as a mainstay of many climate change studies (Panday et al., 2014; Rana et al., 2014; Masood et al., 2015). CMIP5 includes more comprehensive climate models with higher spatial resolutions and richer set of output fields (Taylor et al., 2012).

European region, at first glance, appears to have abundant water resources; however, these resources are distributed unevenly across the region and by taking population density into account, western European countries like Belgium have relatively little water available. Belgium, and particularly the Flanders and Brussels region, with dense population and intensive industrial activity has relatively high levels of water exploitation compared with availability (high water exploitation index). Exploitation of more than 30% of renewable water resources in Belgium (EEA, 2010) underscores the necessity to study the future change in water resources in the country.

* Corresponding author.
E-mail addresses: tabari.ho@gmail.com, hossein.tabari@bwk.kuleuven.be (H. Tabari).

http://dx.doi.org/10.1016/j.gloplacha.2015.05.012
0921-8181/

Table 1
CMIP5 GCMs and number of runs per model used for precipitation analysis (194 runs).

No.	Model	Historical	RCP2.6	RCP4.5	RCP6.0	RCP8.5
1	ACCESS 1.0	1	–	1	–	1
2	ACCESS 1.3	1	–	1	–	1
3	BCC-CSM1.1	3	–	–	–	–
4	BCC-CSM1.1(m)	1	1	1	1	1
5	BNU-ESM	1	1	1	–	1
6	CanESM2	5	5	5	–	5
7	CMCC-CM	1	–	1	–	1
8	CMCC-CMS	1	–	1	–	1
9	CMCC-CESM	1	–	–	–	1
10	CNRM-CM5	1	1	1	–	1
11	CSIRO-MK3.6.0	10	10	10	10	10
12	FGOALS-G2	1	1	1	–	1
13	GFDL-CM3	2	1	1	1	1
14	GFDL-ESM2G	1	1	1	1	1
15	GFDL-ESM2M	1	–	1	1	1
16	GISS-E2-H	2	–	–	–	–
17	GISS-E2-R	3	–	2	–	–
18	HADGEM2-CC	3	–	1	–	1
19	HADGEM2-ES	1	1	–	–	–
20	INM-CM4	1	–	–	–	1
21	IPSL-CM5A-LR	4	–	3	1	3
22	IPSL-CM5A-MR	1	1	1	1	1
23	IPSL-CM5B-LR	1	–	1	–	1
24	MIROC-ESM	1	1	1	1	1
25	MIROC-ESM-CHEM	1	1	1	1	1
26	MIROC5	3	2	1	1	3
27	MPI-ESM_LR	1	1	1	–	1
28	MPI-ESM_MR	1	1	1	–	1
29	MRI-CGCM3	1	1	1	1	1
30	NorESM1-M	3	1	1	1	1

In this context, this work aims to investigate future surface water availability for central Belgium based on the CMIP5 GCMs. To this end, the present-day simulations for two water balance components of precipitation and potential evapotranspiration (estimated by a calibrated version of the Penman method (Bultot et al., 1983)) are validated and then the projections for these variables and water availability under four emission scenarios are presented. Apart from providing the future water availability for the region, this study updates the previous climate scenarios for precipitation and potential evapotranspiration (Baguis et al., 2010; Ntegeka et al., 2014) by assessing new CMIP5 model capabilities.

Table 2
CMIP5 GCMs and number of runs per model used for potential evapotranspiration analysis (>600 runs).

No.	Model	Historical	RCP2.6	RCP4.5	RCP6.0	RCP8.5
1	ACCESS 1.0	–	–	1	–	–
2	ACCESS 1.3	–	–	1	–	–
3	BCC-CSM1.1(m)	–	1	1	1	1
4	BNU-ESM	1	1	1	–	–
5	CanESM2	–	–	–	–	5
6	CNRM-CM5	1	–	1	–	1
7	GFDL-CM3	1	1	–	1	1
8	GFDL-ESM2G	1	1	1	1	1
9	GFDL-ESM2M	1	–	1	1	1
10	HADGEM2-CC	2	–	1	–	–
11	HADGEM2-ES	1	–	–	–	–
12	INM-CM4	1	–	1	–	–
13	IPSL-CM5A-LR	1	3	–	1	3
14	IPSL-CM5A-MR	3	1	–	1	1
15	IPSL-CM5B-LR	1	–	–	–	–
16	MIROC-ESM	3	1	1	1	1
17	MIROC-ESM-CHEM	1	1	1	1	1
18	MIROC5	2	–	3	2	3
19	MRI-CGCM3	1	1	1	–	1

Table 3
Summary of required equations for potential evapotranspiration estimation.

Parameter	Mathematical expression	Notation definition
Total radiation balance (Q_0^*)	$Q_0^* = (1 - \alpha_0)K_s - L$	α_0 = Free water surface albedo K_s = Global solar radiation L = Vaporization latent heat of water
Saturated water vapor pressure gradient (δ)	$\delta = \left(\frac{d\varepsilon}{dT}\right)_T$	$d\varepsilon$ = Saturation deficit T = Air temperature
Psychrometric coefficient (γ)	$\gamma = 0.000662p$	p = Mean atmospheric pressure
Free water surface albedo (α_0)	$\alpha_0 = 0.07 + (A - 0.07)Ir^{0.4}$	A = Albedo of the free water surface under clear sky Ir = Relative insolation
Net terrestrial radiation (L^*)	$L^* = \sigma T^4\left(1-(a+b\sqrt{e})\left(1+c\,(1-Ir)^2\right)\right)$	σ = Stefan–Boltzmann constant T = Air temperature e = Water vapor pressure a, b and c = Location specific parameters (they are determined by measurements on radiation variables)

2. Materials and methods

2.1. Data

General circulation model (GCM) outputs from the phase 5 of the CMIP multi-model database (Taylor et al., 2012) are used in this study. The CMIP5 simulations were used for the fifth assessment report (AR5) of the Intergovernmental Panel on Climate Change (IPCC) and include 4 future emission scenarios called "representative concentration pathways" (RCPs) (Moss et al., 2010; Van Vuuren et al., 2011). In contrast to the Special Report on Emissions Scenarios (SRES), the RCPs are not based on storylines defining the drivers behind the emissions. Rather, the RCPs are defined by selecting concentration pathways and the associated radiative forcing in 2100 so as to cover the full range of scenarios available in the scientific literature. The radiative forcing is a measure of the imbalance of incoming and outgoing energy in the earth–atmosphere system, due to climate altering factors. The RCPs

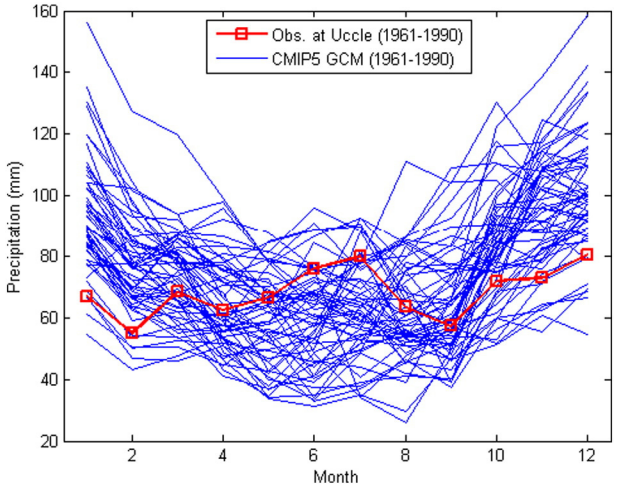

Fig. 1. Mean monthly precipitation for the different CMIP5 GCM control runs (1961–1990).

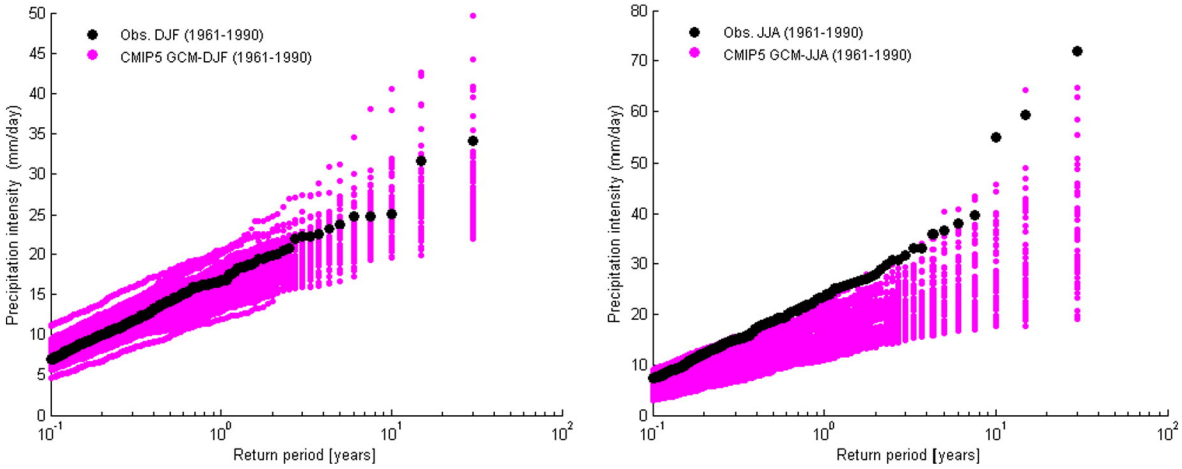

Fig. 2. Wet day precipitation intensities vs. return period: validation of CMIP5 GCM runs based on Uccle historical observations (1961–1990), for winter (left) and summer (right) seasons.

are referenced by the radiative forcing reached in 2100, namely RCP8.5 (8.5 W/m^2, representing the largest emissions or high reference position), RCP6.0, RCP4.5, and RCP2.6 (or RCP3-PD). In the name of the "RCP3-PD" scenario, PD stands for Peak-and-Decline: rather than increasing then stabilizing to a certain value, the radiative forcing is passing through a peak (at 3 W/m^2), then declining and eventually stabilizing (the radiative forcing in 2100 was set to 2.6 W/m^2 following an evaluation of the plausibility of such low scenarios). The two lower scenarios are in the range of concentrations typical for mitigation scenarios, and the lowest one is representative of emissions that would follow from substantial mitigation efforts compatible with a limitation of global warming around 2 °C, so that the coverage of possible futures is much more comprehensive than with the non-mitigation SRES scenarios (Staes et al., 2011).

For this study, the dataset for precipitation and the meteorological variables needed for evapotranspiration estimation for the control (1961–1990) and scenario (2071–2100) periods are obtained from 30 and 19 GCMs, respectively. All the GCMs and their respective number of runs for precipitation and evapotranspiration analyses are listed in Tables 1 and 2, respectively. The CMIP5 GCM outputs were statistically processed and evaluated by comparison with the historical observations at Uccle station. This was done for the GCM grid cell covering that station. This station operated by the Royal Meteorological Institute of Belgium (KMI) is the main meteorological station in Belgium.

2.2. Methodology

A calibrated version of the Penman method (Penman, 1948) for Belgium (Bultot et al., 1983) was used for estimation of daily potential evapotranspiration. In this method, the potential evapotranspiration of a natural cover i is given by:

$$ET_{o_i} = f \times E \tag{1}$$

where ET_{o_i} is potential evapotranspiration (mm/day), f is a transfer coefficient and E is evaporation of a free water surface (mm/day). The evaporation and transfer coefficient are calculated as follow:

$$E = \frac{\delta Q_0^*/L + \gamma(\alpha + \beta u)(\varepsilon\text{-}e)}{\gamma + \delta} \tag{2}$$

$$f = \frac{(1\text{-}\alpha_i)K_s\text{-}L^*}{(1\text{-}\alpha_0)K_s\text{-}L^*} \tag{3}$$

where Q_0^* *is the total radiation balance (J/cm^2 day), L is the vaporization latent heat of water (10^{-4} J/kg), γ is the psychrometric coefficient (hPa/K), α and β are wind factors, u is the mean daily wind speed at 2 m height (km/h), δ is the saturated water vapor pressure gradient, $(\varepsilon - e)$ is the saturation deficit (hPa), α_i is the albedo of the natural cover surface, K_s is the global solar radiation (J/cm^2 day), L^* is the net*

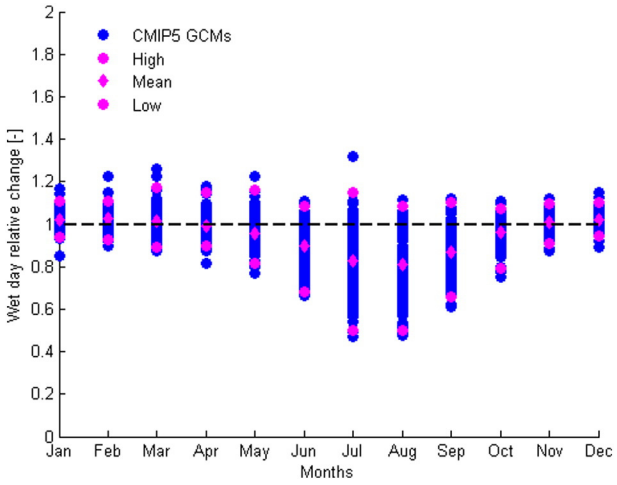

Fig. 3. Change factors in the number of wet days for all RCP scenarios highlighting high, mean and low scenarios.

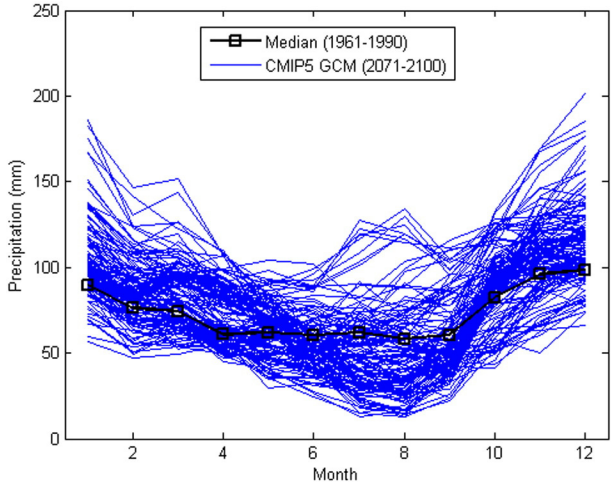

Fig. 4. Mean monthly precipitation for the different CMIP5 GCM future runs (2071–2100), for combined RCP scenarios and median of control runs (1961–1990).

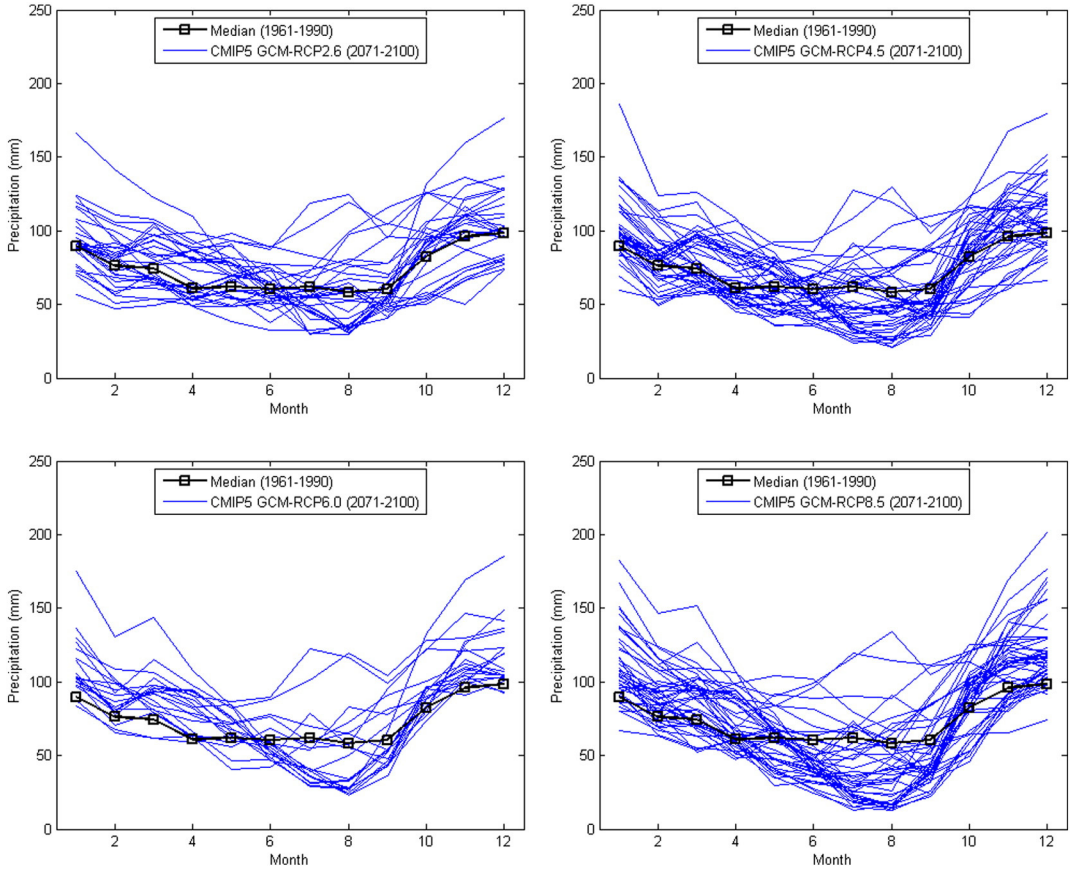

Fig. 5. Mean monthly precipitation for the different CMIP5 GCM future runs (2071–2100), for the individual RCP scenarios and median of control runs (1961–1990).

Table 4
Min–max perturbation (%) of mean seasonal precipitation for the CMIP5 GCM runs, different RCP scenarios, and seasons (MAM: March–April–May; JJA: June–July–August; SON: September–October–November; DJF: December–January–February).

	RCP2.6		RCP4.5		RCP6.0		RCP8.5	
	Max	Min	Max	Min	Max	Min	Max	Min
MAM	24.38	−2.79	23.06	−8.86	16.29	−6.27	40.60	−11.93
JJA	33.44	−36.06	33.56	−48.60	32.97	−38.92	40.73	−53.86
SON	16.53	−8.85	21.21	−12.05	18.41	−7.05	22.45	−13.71
DJF	23.69	−0.38	33.71	−2.47	28.93	−3.88	41.26	−2.02

terrestrial radiation (J/cm^2 day) and α_0 is the free water surface albedo. The required mathematical expressions for these parameters are presented in Table 3.

The estimated potential evapotranspiration as well as precipitation were first analyzed for the current and future periods, and then future water availability was estimated. Monthly/seasonal means and daily quantiles of potential evapotranspiration and precipitation were investigated. Additional analysis for the number of wet days defined as days with precipitation values greater than or equal to 0.1 mm was done. The change in daily quantiles is calculated as ratio between precipitation or potential evapotranspiration values for the scenario

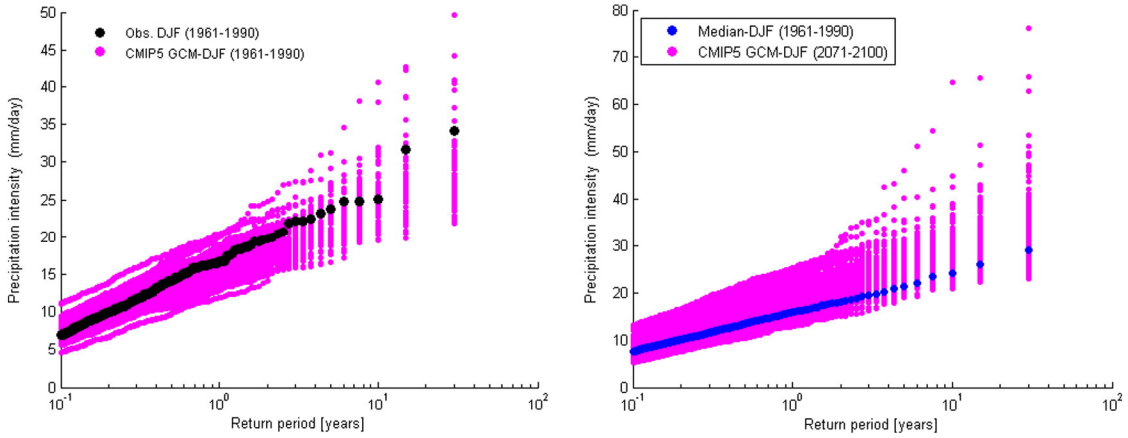

Fig. 6. Wet day precipitation intensities vs. return period: comparison of CMIP5 GCM control (1961–1990) with Uccle observation and scenario (2071–2100) runs with median of control runs, for all RCP scenarios and winter season.

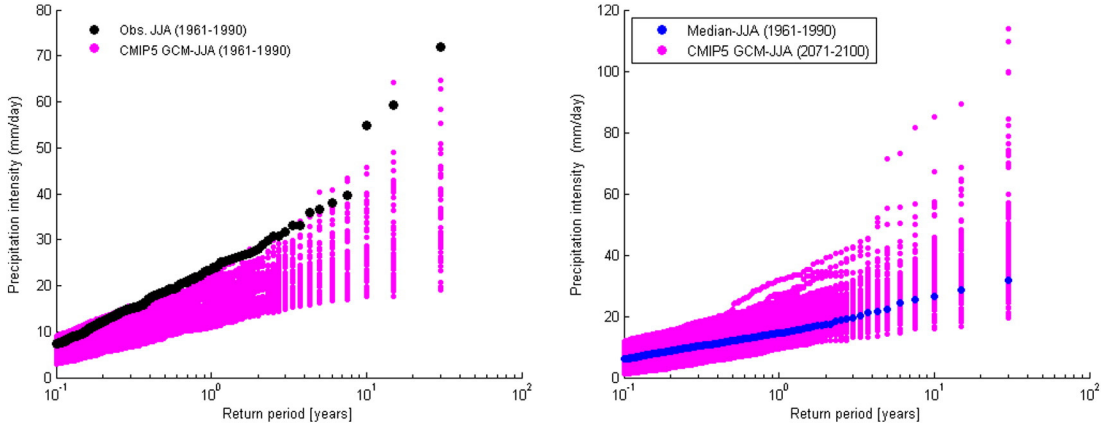

Fig. 7. Wet day precipitation intensities vs. return period: comparison of control (1961–1990) with Uccle observation and scenario (2071–2100) runs with median of control runs, for all RCP scenarios and summer season.

period (2071–2100) and those for the control period (1961–1990) with the same return period (T):

$$RC_{T_i} = \frac{X_S(T_i)}{X_C(T_i)} \tag{4}$$

in which

$$T_i = \frac{N}{i} \tag{5}$$

where RC_{T_i} is the relative change of quantile for a given return period T_i, $X_S(T_i)$ is the quantile for scenario runs, $X_C(T_i)$ is the quantile for control runs, N is the data length (in our case, 30 years for both control and scenario periods) and i is the quantile rank (1 for the highest). In case of the relative change in number of wet days, because the number of wet days for the control and scenario runs might be different, the set of return period values do not coincide and the return periods are derived by linear interpolation from the values with closest return periods. After calculation of the relative changes, high, mean and low climate change scenarios were derived from the entire range of relative changes. The mean scenario was defined as the median of all the relative changes for each return period, and the high and low scenarios as the 5th and 95th percentiles. Same procedure was used for extracting the climate scenarios for a given month, by calculation of the 5th and 95th percentiles and median corresponding each month.

3. Projections for water balance components

3.1. Analysis of precipitation

Prior to analysis of the CMIP5 GCM projections for precipitation and potential evapotranspiration, their simulations for the control period are validated based on the Uccle daily historical observations for the period 1961–1990. Fig. 1 shows the comparison of the mean monthly precipitation depths for the different CMIP5 GCM control runs (1961–1990) and the historical observations at Uccle. When the whole range of model results are evaluated, some systematic overestimations are shown in some of the winter months and a slight systematic underestimation during the summer months. The observed values are, however, located inside the range of model results. The validation of the wet day precipitation intensities versus return period for the winter and summer seasons are shown in Fig. 2. It is shown that the winter precipitation quantiles are nearly unbiased, whereas for the summer season the precipitation extremes are systematically underestimated. Almost all GCM runs for summer season show precipitation quantiles lower than the historical ones. This is because of the coarse resolution of the GCMs; many summer precipitation extremes are due to small scale convective rain storms and these are not explicitly resolved at spatial scales smaller than about 3–4 km (Willems et al., 2012; Kooperman et al., 2014).

After validation of the GCM runs, analysis was made for the climatic change signals as obtained from comparing the scenario versus the control runs from all models. These climatic changes reflect the changes from the reference period 1961–1990 to the future scenario period 1971–2100. Results are summarized for the winter

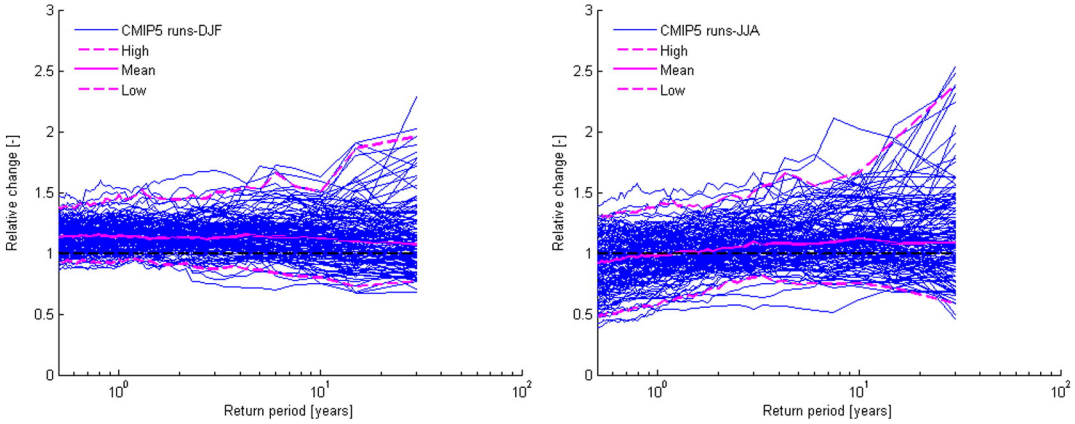

Fig. 8. Wet day relative change calculated based on control (1961–1990) and scenario (2071–2100) runs versus return periods, for all RCP scenarios and winter season (left) and summer season (right).

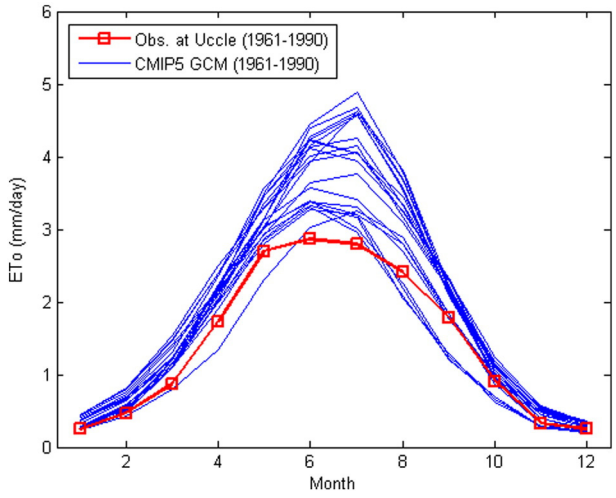

Fig. 9. Mean monthly ET_o for the different CMIP5 GCM control runs (1961–1990).

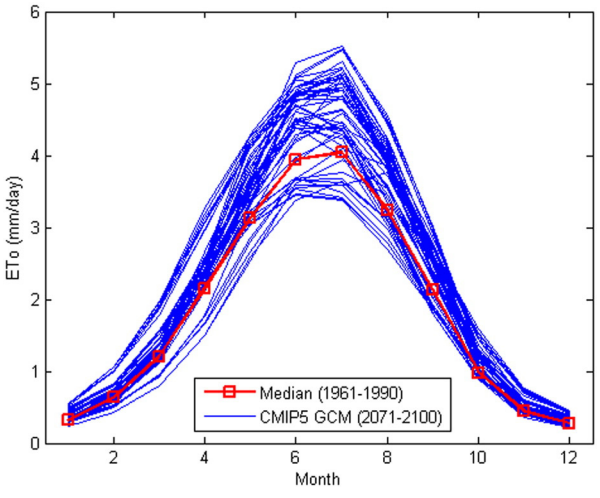

Fig. 11. Mean monthly ET_o for the different CMIP5 GCM future runs (2071–2100), for combined RCP scenarios and median of control runs (1961–1990).

(December–January–February: DJF) and summer (June–July–August: JJA) seasons. The changes in the number of wet days were computed after counting these days in the control and scenario periods for each climate model run. This was done at monthly time scale and the results are summarized as change factors in Fig. 3. The change factors are computed as the ratio of the number of wet days during scenario and control periods. The empirical high, mean and low scenarios are also indicated. The range of the projected wet day changes is wider for the summer months especially for July where these changes range from −53% to 32%, while the narrowest range is projected for the winter season. The number of wet days in the summer period is projected to decrease in most of the scenarios while the projections show increase in the number of wet days for the winter months. By taking the mean change factor, one can see that the change in the months between May and October is higher than that in the months between November and April. This shows the summer months to be drier in the future. From the four scenarios, RCP8.5 is the one that shows the driest conditions.

Fig. 4 shows the comparison of the mean monthly precipitation depths for the different CMIP5 GCM scenario runs (2071–2100) and the median of GCM control runs (1961–1990). When the future projections are compared with the median of the control runs, it is shown that the winter becomes wetter and the summer gets drier. The results for the individual RCP scenarios are shown in Fig. 5. The same trends are shown for each of the scenarios, but the trends are stronger for the higher concentration scenarios (highest changes for RCP8.5 scenario, lowest changes for RCP2.6). Table 4 summarizes the range of the changes in mean seasonal precipitation depths, by their minimum and maximum values for the different RCP scenarios and seasons. The mean seasonal changes go as high as +41% for the winter season for the RCP8.5 scenario, and down to −54% for the summer season for the same scenario. For the other scenarios, the changes are lower.

Figs. 6 and 7 show the differences in wet day precipitation depths versus return period, between the CMIP5 GCM control and scenario runs. It is seen in the figures that the precipitation extremes increase both in winter and summer seasons. The projected change factors (relative changes) for the winter (DJF) and summer (JJA) seasons are shown in Fig. 8. The daily relative change factors were obtained for the rainfall quantiles that correspond to the highest 300 daily rainfall intensities in the 30-year runs (hence for return periods > 0.1 year) and the high, mean and low scenario changes were identified. It can be seen that the range of change is wider for the summer season compared to that of the winter season. These factors also illustrate that the changes for the summer season increase for higher return periods, whereas the changes are approximately constant (independent of the return period) for the winter season.

3.2. Analysis of potential evapotranspiration

Mean monthly values of ET_o for GCM control runs and the values observed at Uccle station are shown in Fig. 9. As one can see, all of the climate models can capture the inter-annual variation of ET_o. The observed and climate models' simulated ET_o values follow similar pattern. In terms of magnitude, most of the climate model runs systematically overestimate the mean monthly ET_o values especially for summer. The

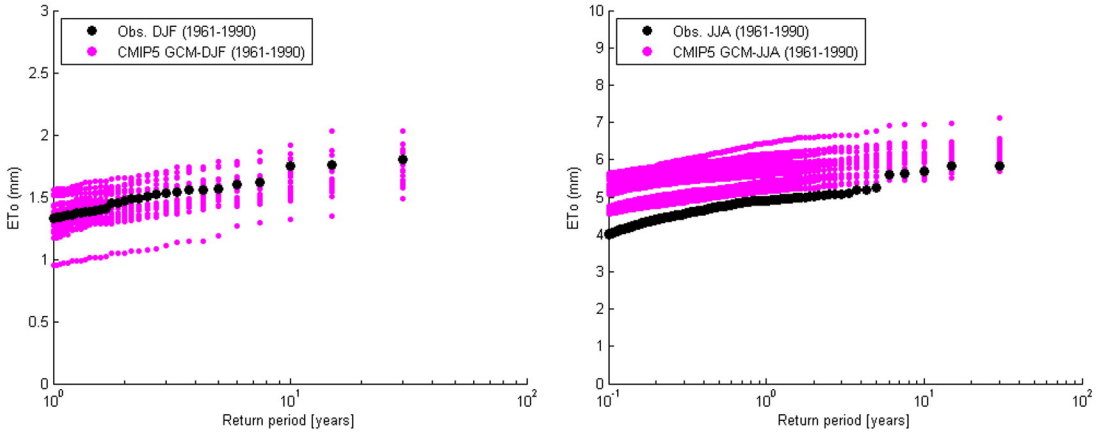

Fig. 10. Evapotranspiration vs. return period: validation of CMIP5 GCM runs based on Uccle historical observations (1961–1990), for winter (left) and summer (right) seasons.

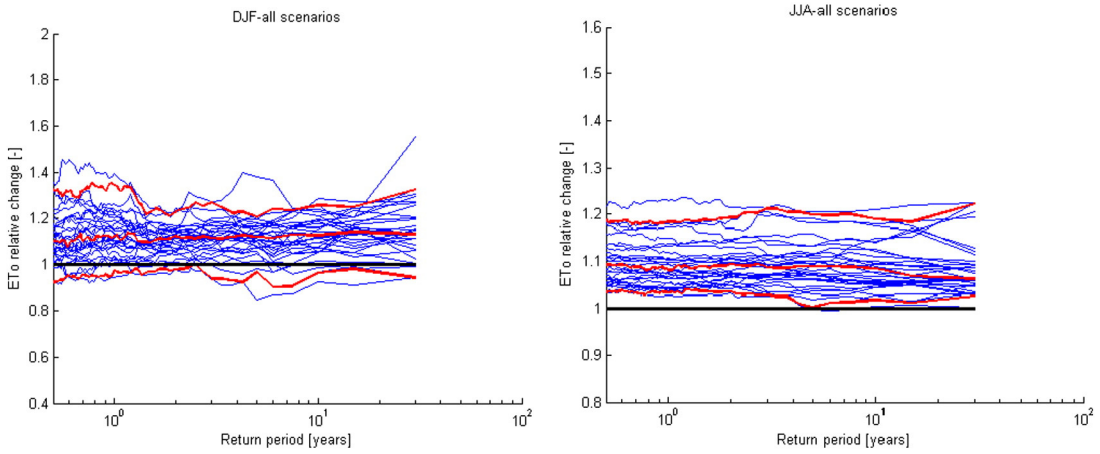

Fig. 12. ET_o change factors vs. return period for the different CMIP5 GCM runs, all RCP scenarios combined, for winter (left) and summer (right) seasons.

variation of daily ET_o for winter and summer seasons is illustrated in Fig. 10. It is found that summer ET_o values are overestimated by almost all climate models, while half of the models overestimate winter ET_o values.

Similar to precipitation analysis, the ET_o projections are analyzed after validating the current climate simulations. Compared to the median of the control runs, most GCM runs project higher increase in ET_o for the 2071–2100 horizon. Fig. 11 shows the mean monthly ET_o for all the RCP scenarios comparing with the median of the control runs. The projected changes are calculated for ET_o based on control and scenario period runs. The change factors are calculated similar to precipitation. The results for winter and summer season are shown in Fig. 12. During the winter season, the quantiles with higher return periods show a wider range than the quantiles with lower return periods. Compared to the summer season, the magnitude of change in the winter season is smaller. The changes are approximately constant (independent on the return period).

Considering the future increase in evapotranspiration for both winter and summer seasons, a sensitivity analysis was carried out to understand which meteorological variables are responsible for the evapotranspiration increase projected by the CMIP5 GCMs. In order to explore the possible causes behind such increase in evapotranspiration by the CMIP5 GCMs, the CMIP5 GCM evapotranspiration changes due to change in each meteorological variable were studied based on the output of the climate model with the highest evapotranspiration change (i.e., GFDL-CM3 model's data under RCP8.5 scenario). The results are presented in Table 5. As the results indicate, an increase in mean temperature is responsible for about 60% and 57% of the observed changes in evapotranspiration in the winter and summer seasons, respectively. An increase in solar radiation is the other main factor associated with the increased evapotranspiration. The contributions of mean temperature and solar radiation to evapotranspiration change are also evident in Fig. 13. The changes in evapotranspiration are moreover highly influenced by changes in maximum and minimum temperatures especially during the winter season. The effects of the other meteorological variables on the evapotranspiration changes except for relative humidity in winter are negligible. The insignificant effect of wind speed on evapotranspiration in humid climates was also

Table 5
Percent changes in daily evapotranspiration (return period > 0.1 years) due to change in each meteorological variable based on GFDL-CM3 model's data under RCP8.5 scenario.

	Mean temperature	Maximum temperature	Minimum temperature	Solar radiation	Relative humidity	Wind speed	Air pressure
Winter	59.72	17.68	15.29	14.97	−8.97	1.53	−0.29
Summer	56.74	12.48	7.94	24.30	−1.13	−0.74	−0.30

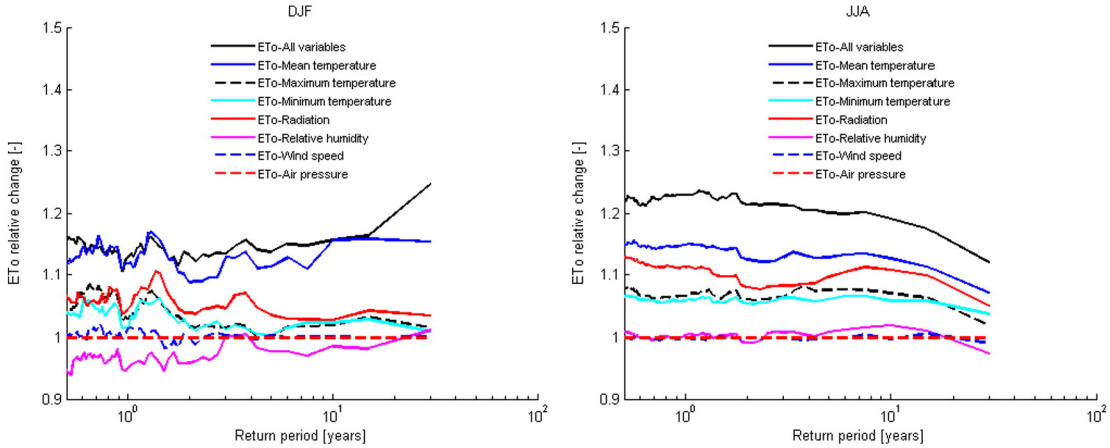

Fig. 13. Sensitivity analysis of evapotranspiration (ET_o) change due to individual variables for winter and summer.

Table 6
Estimated sensitivity coefficients for air temperatures and solar radiation variables based on GFDL-CM3 model's data under RCP8.5 scenario.

	Mean temperature	Maximum temperature	Minimum temperature	Solar radiation
Winter	0.09	0.05	0.01	0.07
Summer	0.19	0.07	0.03	0.12

reported by Irmak et al. (2006) and Tabari and Hosseinzadeh Talaee (2014). In general, it can be inferred that the main factors associated with evapotranspiration increase are air temperature and solar radiation. The sensitivity of evapotranspiration to mean temperature and solar radiation variables is also investigated in terms of sensitivity coefficients (Table 6). The analysis indicates sensitivity coefficients of 0.19 and 0.09 for summer and winter mean temperatures, respectively. This means that a 10% increase in summer and winter mean temperature values, while other variables required for evapotranspiration calculation are held constant, may increase evapotranspiration by 1.9% and 0.9%, respectively. Furthermore, the obtained sensitivity coefficients of 0.12 and 0.07 for summer and winter solar radiation imply that a 10% increase in summer and winter solar radiation results in 1.2% and 0.7% increases in evapotranspiration respectively, while all other variables are held constant. The higher sensitivity coefficients of solar radiation and mean temperature compared with those of maximum and minimum temperatures indicate the greater impact of solar radiation and mean temperature on the evapotranspiration estimates.

4. Future water availability

Previous studies at the global scale based on the CMIP3 dataset indicated an increase in future water availability in high-latitude regions (Milly et al., 2005; Arnell and Gosling, 2013), but what will happen for different seasons at the regional scale on the basis of the new CMIP5 GCMs is unknown. Hence, a seasonal water balance analysis was conducted to investigate whether Belgium will move towards increase in precipitation excess in winter and decrease in precipitation excess in summer. This was done by calculating change factors (change from control to future conditions) from the CMIP5 results for precipitation and ET_o, and applying these change factors to the mean monthly precipitation and ET_o values of the current climate conditions based on the Uccle series (delta change method). The change factors were chosen on monthly basis after checking the correlation between precipitation and ET_o changes and by seasonal tracking of the models that give the higher-median-lower changes in specific hydrological conditions, following the approach by Ntegeka et al. (2014) for tailored climate scenario development. The results of the correlation analysis between precipitation and ET_o change are shown in Fig. 14. As the plots show, there is no strong relationship for both winter and summer seasons. For water balance analysis, scenarios were considered that lead to high positive changes in winter and high negative changes in summer. Hence, the factors were considered that correspond to high changes for both precipitation and ET_o for winter season months. For summer season months, factors that correspond to high changes in ET_o and low changes in precipitation were selected. Afterwards, the mean

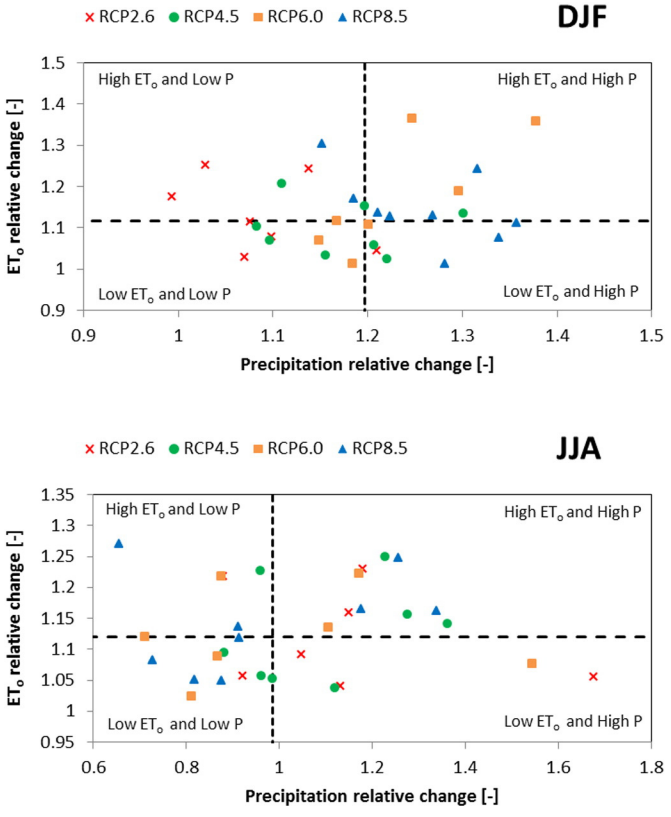

Fig. 14. Inter-seasonal tracing of precipitation and ET_o relative changes (averaged for return periods > 0.1 year) for the different RCP scenarios and for winter (top) and summer (bottom) seasons. The medians are marked with dashed lines.

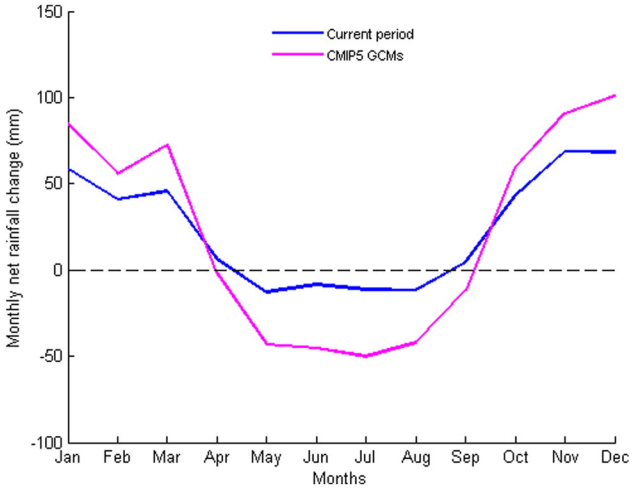

Fig. 15. Net rainfall for control period (1961–1990) and future period (2071–2100) of CMIP5 GCMs, for scenarios that lead to high positive changes in winter and high negative changes in summer.

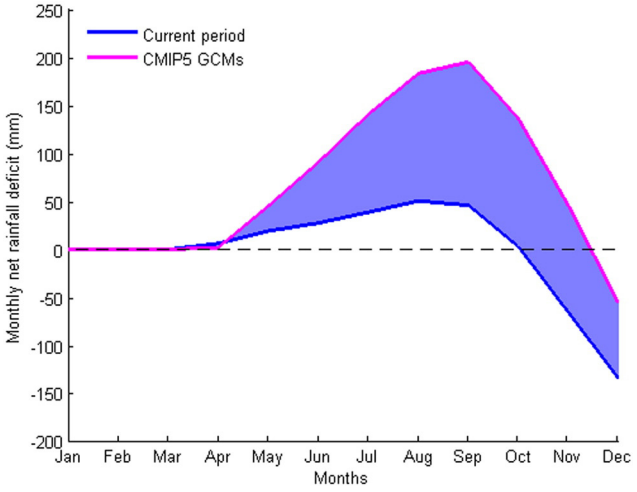

Fig. 16. Net rainfall deficit throughout a year at the end of the century for the scenario that leads to high negative changes in summer.

monthly rainfall excess or net rainfall was computed by subtracting ET_o from precipitation. The results are as shown in Fig. 15 and illustrate that the net rainfall is projected to decrease during summer and increase during winter. The scenarios with the high CMIP5 changes project larger decrease in net rainfall for the summer period. Therefore, severe drier conditions may be expected during summer periods. It means the total water available for runoff, soil water storage may change strongly and subsequently ground water recharge (Schuol et al., 2008) may decrease strongly. Kumar et al. (2014) also showed a general decrease in available water for dry seasons and increasing available water for wet seasons for Western Europe.

The other analysis that was conducted on the net rainfall is obtaining the net rainfall deficit throughout a year (starting at the dry season months) by the end of the century. The results are shown in Fig. 16, using data similar to Fig. 15. As can be seen, the projections by the higher scenarios of the CMIP5 GCMs indicate that the cumulative water shortage is equal to zero during January, February and March, while during the summer season it can go up to about 200 mm. According to this figure, the impact of this water shortage is projected to affect consecutive six months out of the year and the compensation during the winter months may be much less in the future. Okazaki et al. (2012) reported decreases in future water availability in Western Europe with excepted higher increase in evaporation compared with precipitation.

5. Conclusions

This paper presents an assessment of the possible impact of climate change on water availability for central Belgium. Precipitation, potential evapotranspiration and water availability were analyzed using the historical simulations for the period 1961–1990 and the future projections for the period 2071–2100 from the CMIP5 GCMs under the RCP2.6, RCP4.5, RCP6.0 and RCP8.5 emission scenarios. The results show for most models a decrease for number of wet days and mean monthly precipitation for the summer season and an increase for the winter season. For potential evapotranspiration, an increasing trend is projected for both winter and summer seasons. The results also indicate that the water availability for the late 21st century is expected to decrease for summer and increase for winter. In other words, wet season will get wetter and dry season drier, resulting in an increased risk of summer droughts and winter floods in the region. During the summer season, the cumulative water shortage can go up to about 200 mm. This is of high concern particularly for the Flanders and Brussels region of Belgium that is highly vulnerable to reduced water availability because of high population density. It therefore requires attention by the responsible authorities.

Acknowledgments

This study was partly supported by research projects for the Flemish Environment Agency (Division Operational Water Management and Environmental Reporting, project no. VMM/ALMC/MIRA/2013/02), and partly by the Belgian Science Policy Office (BELSPO; BRAIN-be programme, grant no. BR/143/A2/CORDEX.be) and the Research Foundation—Flanders (FWO, grant no. G001311N).

References

Arnell, N.W., Gosling, S.N., 2013. The impacts of climate change on river flow regimes at the global scale. J. Hydrol. 486, 351–364.
Baguis, P., Roulin, E., Willems, P., Ntegeka, V., 2010. Climate change scenarios for precipitation and potential evaporation over central Belgium. Theor. Appl. Climatol. 99, 273–286.
Bates, B.C., Kundzewicz, Z.W., Wu, S., Palutikof, J.P. (Eds.), 2008. Climate change and water. Technical Paper of the Intergovernmental Panel on Climate Change (IPCC Secretariat), p. 210.
Bultot, F., Coppens, A., Dupriez, G., 1983. Estimation de l'évapotranspiration potentielle en Belgique. Publications/publicaties série/serie A, No/Nr 112Institut Royal Météorologique de Belgique - Koninklijk Meteorologisch Instituut van België (28 pp.).
Cisneros, B.E.J., Oki, T., Arnell, N.W., Benito, G., Cogley, J.G., Döll, P., Jiang, T., Mwakalila, S.S., Fischer, T., Gerten, D., Hock, R., Kanae, S., Lu, X., Mata, L.J., Pahl-Wostl, C., Strzepek, K.M., Su, B., van den Hurk, B., 2014. Climate Change 2014: Impacts, Adaptation, and Vulnerability. Contribution of Working Group II to the Fifth Assessment Report of the Intergovernmental Panel on Climate Change. IPCC.
EEA, 2010. The European environment—state and outlook 2010: water resources—quantity and flows. European Environment Agency, Copenhagen.
Irmak, S., Payero, J.O., Martin, D.L., Irmak, A., Howell, T.A., 2006. Sensitivity analyses and sensitivity coefficients of standardized daily ASCE Penman–Monteith equation. J. Irrig. Drain. Eng. 132 (6), 564–578.
Kling, H., Stanzel, P., Preishuber, M., 2014. Impact modelling of water resources development and climate scenarios on Zambezi River discharge. J. Hydrol. Reg. Stud. 1, 17–43.
Kooperman, G.J., Pritchard, M.S., Somerville, R.C.J., 2014. The response of US summer rainfall to quadrupled CO_2 climate change in conventional and superparameterized versions of the NCAR community atmosphere model. J. Adv. Model. Earth Syst. 6, 859–882.
Kumar, S., Lawrence, D.M., Dirmeyer, P.A., Sheffield, J., 2014. Less reliable water availability in the 21st century climate projections. Earth's Future 2, 152–160.
Lins, H.F., Cohn, T.A., 2011. Stationarity: wanted dead or alive? J. Am. Water Resour. Assoc. 47, 475–480.
Masood, M., Yeh, P.J.-F., Hanasaki, N., Takeuchi, K., 2015. Model study of the impacts of future climate change on the hydrology of Ganges–Brahmaputra–Meghna basin. Hydrol. Earth Syst. Sci. 19, 747–770.
Matalas, N.C., 2012. Comment on the announced death of stationarity. J. Water Resour. Plan. Manag. 138, 311–312.
Meehl, G., Stocker, T., Collins, W., 2007. Global Climate Projections. Cambridge Univ Press, Cambridge, UK.
Milly, P.C.D., Dunne, K.A., Vecchia, A.V., 2005. Global pattern of trends in streamflow and water available in a changing climate. Nature 438, 347–350.
Milly, P.C.D., Betancourt, J., Falkenmark, M., Hirsch, R.M., Kundzewicz, Z.W., Lettenmaier, D.P., Stouffer, R.J., 2008. Stationarity Is Dead: Whither Water Management?: Science 319, 573–574.
Moss, R.H., et al., 2010. The next generation of scenarios for climate change research and assessment. Nature 463, 747–756.
Ntegeka, C., Baguis, P., Roulin, E., Willems, P., 2014. Developing tailored climate change scenarios for hydrological impact assessments. J. Hydrol. 508, 307–321.
Okazaki, A., Yeh, P.J.-F., Yoshimura, K., Watanabe, M., Kimoto, M., Oki, T., 2012. Changes in flood risk under global warming estimated using MIROC5 and the discharge probability index. J. Meteorol. Soc. Jpn. 90 (4), 509–524.
Panday, P.K., Thibeault, J., Frey, K.E., 2014. Changing temperature and precipitation extremes in the Hindu Kush-Himalayan region: an analysis of CMIP3 and CMIP5 simulations and projections. Int. J. Climatol. http://dx.doi.org/10.1002/joc.4192.
Penman, H.L., 1948. Natural evaporation from open water, bare and grass. Proc. R. Soc. Lond. A 193, 120–145.
Rana, A., Fostera, K., Bosshard, T., Olsson, J., Bengtsson, L., 2014. Impact of climate change on rainfall over Mumbai using Distribution-based Scaling of Global Climate Model projections. J. Hydrol. Reg. Stud. 1, 107–128.
Schewe, J., Heinke, J., Gerten, D., Haddeland, I., Arnell, N.W., Clark, D.B., Dankers, R., Eisner, S., Fekete, B., Colón-González, F.J., Gosling, S.N., Kim, H., Liu, X., Masaki, Y., Portmann, F.T., Satoh, Y., Stacke, T., Tang, Q., Wada, Y., Wisser, D., Albrecht, T., Frieler, K., Piontek, F., Warszawski, L., Kabat, P., 2014. Multi-model assessment of water scarcity under climate change. Proc. Natl. Acad. Sci. 111. http://dx.doi.org/10.1073/pnas.1222460110.
Schuol, J., Abbaspour, K.C., Yang, H., Srinivasan, R., Zehnder, A.J.B., 2008. Modeling blue and green water availability in Africa. Water Resour. Res. 44, W07406. http://dx.doi.org/10.1029/2007WR006609.
Shifteh Some'e, B., Ezani, A., Tabari, H., 2013. Spatiotemporal trends of aridity index in arid and semi-arid regions of Iran. Theor. Appl. Climatol. 110, 385–393.
Staes, J., Willems, P., Marbaix, P., Vrebos, D., Bal, K., Meire, P., 2011. Impact of climate change on river hydrology and ecology: a case study for interdisciplinary policy oriented research SUDEM-CLI. Final Report. Belgian Science Policy, Brussels (112 pp.).
Tabari, H., Aghajanloo, M.-B., 2013. Temporal pattern of aridity index in Iran with considering precipitation and evapotranspiration trends. Int. J. Climatol. 33, 396–409.
Tabari, H., Hosseinzadeh Talaee, P., 2013. Moisture index for Iran: spatial and temporal analyses. Glob. Planet. Chang. 100, 11–19.
Tabari, H., Hosseinzadeh Talaee, P., 2014. Sensitivity of evapotranspiration to climatic change in different climates. Glob. Planet. Chang. 115, 16–23.
Taylor, K.E., Stouffer, R.J., Meehl, G.A., 2012. An overview of CMIP5 and the experiment design. Bull. Am. Meteorol. Soc. 93, 485–498.
van Vuuren, D.P., et al., 2011. RCP2.6: exploring the possibility to keep global mean temperature increase below 2 °C. Clim. Chang. 109, 95–116.
Willems, P., Arnbjerg-Nielsen, K., Olsson, J., Nguyen, V.T.V., 2012. Climate change impact assessment on urban rainfall extremes and urban drainage: methods and shortcomings. Atmos. Res. 103, 106–118.